



Power Electronic Systems
Laboratory

© 2014 IEEE

Proceedings of the International Power Electronics Conference - ECCE Asia (IPEC 2014), Hiroshima, Japan, May 18-21, 2014

Control Method for Inductive Power Transfer with High Partial-Load Efficiency and Resonance Tracking

R. Bosshard,
J. W. Kolar,
B. Wunsch

This material is published in order to provide access to research results of the Power Electronic Systems Laboratory / D-ITET / ETH Zurich. Internal or personal use of this material is permitted. However, permission to reprint/republish this material for advertising or promotional purposes or for creating new collective works for resale or redistribution must be obtained from the copyright holder. By choosing to view this document, you agree to all provisions of the copyright laws protecting it.



Eidgenössische Technische Hochschule Zürich
Swiss Federal Institute of Technology Zurich

Control Method for Inductive Power Transfer with High Partial-Load Efficiency and Resonance Tracking

R. Bosshard*, J. W. Kolar*, and B. Wunsch†

*Power Electronic Systems Laboratory, ETH Zürich, Switzerland, Email: bosshard@lem.ee.ethz.ch

†ABB Switzerland Ltd., Corporate Research, 5405 Baden-Dättwil, Switzerland

Abstract—Frequency controlled Inductive Power Transfer (IPT) systems for Electric Vehicle (EV) battery charging applications often suffer from high power losses in partial-load, because the transmitter coil current is not significantly reduced at low output power. Therefore, in this paper a novel control method is presented that exhibits a substantially higher partial-load efficiency, while it also enables full control of the power semiconductor switching conditions. The power flow control is based on the dynamic regulation of the dc-link voltages on both sides of the resonant system with dc-dc-converters. Additionally, a tracking of the resonance with a current zero crossing detection circuit and a PLL makes the switched current an additional degree of freedom, that can be used, e.g., for the minimization of IGBT soft-switching losses due to stored-charge. All calculated results are supported by experimental measurements on an existing 5 kW/52 mm air gap/210 mm coil diameter prototype system with an efficiency of more than 96.5% at maximum power and above 96% down to 20% rated power.

I. INTRODUCTION

Inductive Power Transfer (IPT) is widely discussed as a battery charging technology for Electric Vehicles (EV), because of the considerable simplification of the charging process due to the contactless transmission of the charging energy. It has been shown in recent publications that with an appropriately designed system a dc-to-dc efficiency comparable to conventional chargers with direct electrical connection can be achieved [1]–[4]. However, additional requirements for the battery charging system arise from the employed battery technology, which have not yet been fully addressed in literature on IPT systems.

For an efficient and fast charging of the lithium-ion batteries, which are commonly used in modern EVs, because of their high energy density, Constant Current/Constant Voltage (CC/CV) charging profiles similar to **Fig. 1** are typically used. Hence, a substantial part of the charging process does not require the full output power from the converter, especially when the State-of-Charge (SoC) is close to the allowed maximum and the current must be reduced to protect the cells from over-charging. Therefore, apart from the efficiency at the nominal point, for a battery charging system also the efficiency in partial-load is of importance. For IPT charging systems with vehicle-to-grid capabilities [4]–[6] the efficiency in partial-load is even more important to make bi-directional energy exchange with the grid financially and ecologically attractive. However, the optimization of a resonant converter system, such as an IPT system, for more than one operating point is highly challenging. Depending on the used control method, reactive currents in the IPT coil windings cause high losses in partial-load which reduce the efficiency dramatically. Therefore, in this paper it is shown that by dynamically adapting the dc-link voltage to the load conditions with two additional dc-dc-converters on both sides of the IPT link, the efficiency can be increased substantially.

In a practical IPT system additional requirements for the control arise from parameter uncertainties. Apart from coil misalignment,

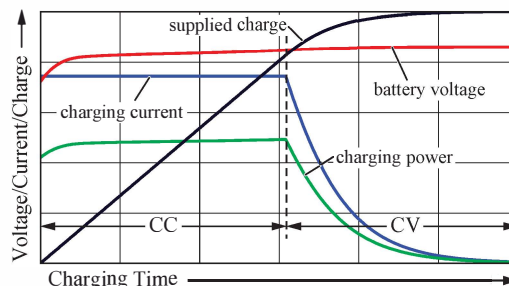


Fig. 1. Typical CC/CV charging profile for EV Li-ion battery cells.

which is widely discussed in literature, also component tolerances and temperature drift are influencing the voltage gain and the resonant frequency of an IPT system. The control method presented in this paper incorporates an automatic tracking of the resonant frequency and dynamic compensation of the varying gain. As an additional feature, the novel control method provides full control over the switching conditions of the transmitter-side power semiconductors. This is particularly important for IPT battery charging systems employing IGBTs as switches to transmit power in the range of several tens of kilowatts. Due to the stored charge of IGBTs [7]–[10] high soft-switching losses occur despite close-to-zero current switching. Because the current at the turn-off instant of the IGBT is a degree of freedom of the presented control method, it enables highest efficiencies for high-power IPT battery charging systems.

The paper is divided into five sections: in Section II insight into the design of a 5 kW IPT system with a focus on controllability is given. Existing control methods are discussed in Section III and a novel control method is presented in Section IV. A comparison of the described existing and the novel control method based on experimental measurements is included. The improved performance of the novel control method is achieved at the cost of additional volume and losses of an additional dc-dc-converter. Therefore, the efficiency requirements and design aspects for the dc-dc-converter are discussed in Section V. Concluding remarks are given in Section VI.

II. IPT SYSTEMS FOR BATTERY CHARGING

In [2], [3], the design of a 5 kW/52 mm air gap/210 mm coil diameter IPT system with a dc-to-dc efficiency of 96.5% was presented. The main specifications of the IPT prototype are given in **Tab. I**. This system is also used for the experiments in this paper. Therefore, in this section a brief overview of the control-related design aspects of the system is given and requirements for an IPT controller are derived.

A. Design Rules for SS-Compensation

As discussed in [3], the design rules for a series-series compensated IPT system as shown in **Fig. 2(a)** for maximum transmission

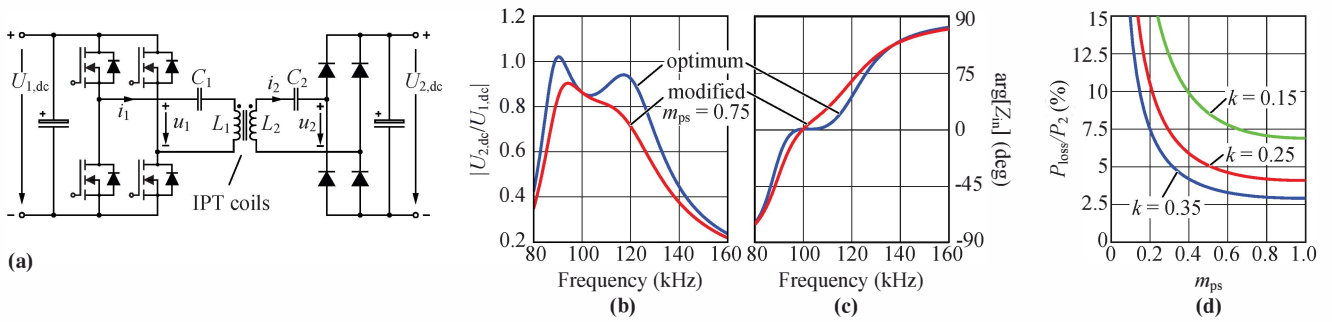


Fig. 2. (a) Equivalent circuit diagram of a series-series compensated IPT system; (b) transfer function from the input to the output dc-link voltage and (c) phase angle of the input impedance of a system designed according to the design rules of [3] and for a system with parameters that were modified with $m_{ps} = 0.75$ to avoid pole-splitting; (d) total loss factor P_{loss}/P_2 as a function of the factor m_{ps} .

Table I

SPECIFICATIONS OF THE PROTOTYPE IPT SYSTEM IN [3], WHICH IS USED FOR THE PRESENTED EXPERIMENTS.

Var.	Value	Description
P_2	5000 W	output power
$U_{1,dc}$	400 V	transmitter-side dc-link voltage
$U_{2,dc}$	350 V	receiver-side dc-link voltage
U_{batt}	350 V	battery voltage
δ	52 mm	air gap
D_c	210 mm	coil diameter
f_0	100 kHz	transmission frequency
α	1.47 kW/dm ²	power density
η	96.5%	max. dc-to-dc efficiency

efficiency at the angular resonant frequency $\omega_0 = 2\pi f_0$ are

$$\omega_0 L_2 \approx \frac{R_{L,eq}}{k_0} \quad (1)$$

for the reactance of the receiver coil and

$$L_1 = L_2 \left(\frac{U_{1,dc}}{U_{2,dc}} \right)^2 \quad (2)$$

for the transmitter coil self-inductance, where k_0 denotes the magnetic coupling at the nominal position of the coils. This design ensures an optimal matching of the receiver coil to the equivalent resistance of the load at the nominal point, which is given by

$$R_{L,eq} = \frac{8}{\pi^2} \frac{U_{2,dc}^2}{P_2}. \quad (3)$$

for a diode rectifier with a capacitive output filter [11].

The resonant frequency is set by choosing the capacitances for the transmitter and the receiver side resonant compensation as

$$C_1 = \frac{1}{\omega_0^2 L_1} \quad \text{and} \quad C_2 = \frac{1}{\omega_0^2 L_2}. \quad (4)$$

These design rules are discussed in detail and experimentally verified in [3]. The focus of this paper is the controllability of the system. Therefore, in the next part, the transfer characteristics are discussed and it is shown how they are influenced by capacitor tolerances and temperature drift. Based on the discussion, requirements for a controller are derived.

B. Transfer Characteristics

The transfer function from the input to the output dc-link voltage is shown in **Fig. 2(b)**. For a system design based on the guidelines

above, a pole-splitting occurs and the voltage transfer function exhibits the two peaks that are characteristic for this phenomenon [12], [13]. At the same time, the phase angle of the input impedance seen from the transmitter-side shown in **Fig. 2(c)** has a saddle point at the resonant frequency.

These transfer characteristics are undesired, because they cause

- i) hard-switching of the transmitter-side power semiconductors during operation close to the resonant frequency
- ii) non-monotonous transfer behavior that may lead to instability of a variable frequency controller

Power losses due to hard-switching (i) of the power semiconductors are of highest concern. Because of the small (or even negative) phase angle between voltage and current at the transmitter-side terminals of the resonant circuit, the current at the switching instants of the power semiconductors can be insufficient to completely discharge the output capacitance of the MOSFET that is turned on. Therefore, Zero Voltage Switching (ZVS) is no longer achieved, because the remaining charge in the output capacitance is dissipated in the MOSFET during the turn-on transition. If IGBTs are used instead, the soft-switching losses due to the stored charge in the junction [8]–[10] similarly impair the performance of the converter, as is discussed in more detail in Section IV.

As shown in later parts of this paper, typically the frequency characteristic of the resonant circuit is exploited to regulate the power flow in the IPT system. In this case, the non-monotonous shape of the voltage transfer function (ii) may cause instability of conventional PID-controllers or could cause convergence to an undesired operating point far above the resonant frequency.

For these reasons a pole-splitting is best avoided by the design process. However, as discussed in [12], for the series-series compensated system a pole-splitting occurs as soon as the magnetic coupling is higher than the limit value

$$k_{lim} = \frac{R_{L,eq}}{\omega_0 L_2}. \quad (5)$$

Unfortunately, this coincides with the design rule (1) that is required to reach the physical maximum transmission efficiency. Hence, a pole-splitting can only be avoided at the cost of additional losses in the IPT coils.

A straight-forward solution is to avoid a pole-splitting by reducing the self-inductance of the receiver coil by a factor m_{ps} below the optimum value

$$L'_2 = m_{ps} L_2, \quad (6)$$

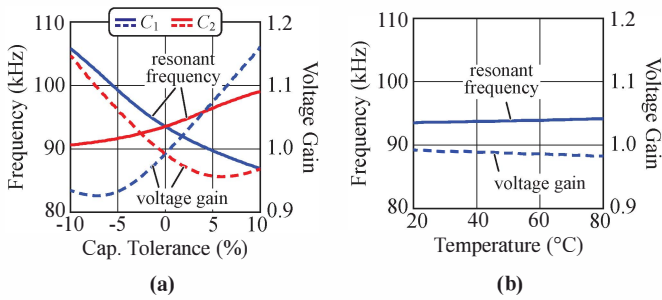


Fig. 3. (a) Influence of capacitor tolerance and (b) temperature drift on the IPT system in [3], which must be compensated by the control.

which increases the limit value k_{lim} by m_{ps}^{-1} . In order to provide the same voltage transfer ratio at the resonant frequency,

$$|G_v(\omega_0)| = \left| \frac{U_{2,dc}}{U_{1,dc}} \right| = \frac{R_{L,eq}}{\omega_0 L_h}, \quad (7)$$

the mutual inductance L_h must remain constant. This is achieved by adapting the self-inductance of the transmitter coil as $L'_1 = L_1/m_{ps}$. The resonant capacitances are adapted to the corrected self-inductance values according to (4). The resulting voltage transfer function and the phase angle of the input impedance for $m_{ps} = 0.75$ are shown in **Fig. 2(b)-(c)**.

The price that has to be paid for the improved controllability and reduced switching losses can be calculated as a function of the factor m_{ps} from the total loss factor P_{loss}/P_2 given in [1], [3], which is shown in **Fig. 2(d)**. Owing to the relatively flat minimum of the total loss factor, a correction with $m_{ps} = 0.75$ causes only few additional losses and is, therefore, acceptable.

Note that the pole-splitting may occur either if the magnetic coupling becomes larger than k_{lim} , e.g., because the IPT coils are placed closer together, or if the equivalent load resistance $R_{L,eq}$ becomes low enough that k_{lim} increases until it exceeds the magnetic coupling. Because a low equivalent resistance corresponds to a high output power (or a low receiver-side dc-link voltage), the IPT system has to be designed with the discussed design rules for the maximum expected magnetic coupling and the maximum output power. Then, even if during operation the magnetic coupling is reduced below the nominal value or if the output power is decreased, no pole-splitting will occur.

C. Requirements for the Control

The key requirement for an EV battery charging system is a tight control of the battery current according to a CC/CV charging profile similar to **Fig. 1**. Additionally, the battery temperature and the SoC must be constantly monitored and the applied current and voltage must be limited in order to prevent damage of the battery, due to excessive heat generation or over-charging. Preferably, these tasks are mainly executed on the receiver side of the IPT system, because this allows shorter reaction times than what could be achieved via a wireless communication across the air gap.

The task of the transmitter is to operate the IPT system under optimum conditions and the supply of the charging power. For lowest switching losses in the transmitter-side power electronics, a controller for the modified IPT system must be able to guarantee operation in the inductive region of the input impedance (cf. **Fig. 2(c)**). However, the actual resonant frequency is an uncertain parameter which needs to be determined by the control in real time.

For an industrially produced IPT system, the effect of capacitance tolerances shown in **Fig. 3(a)** has to be considered. Given (4), a

mis-match in capacitance has an effect on the resonant frequency. However, also the voltage gain (7) is considerably affected if the transmitter-side and receiver-side resonant circuits are no longer tuned to the same frequency. Additionally, **Fig. 3(a)** shows that depending on which capacitor is afflicted by production tolerances, the voltage gain may be increased or reduced. Thus, a control margin in both directions must be included in the design.

Fig. 3(b) shows an estimate of the influence of the operating temperature on the resonant frequency and the voltage gain. To model the effect of temperature drift, the temperature dependency of typical core material (N87) and of polypropylene film capacitors with metallized plastic film (MKP) have been approximated based on the data given in [14], [15]. A temperature coefficient of 0.0039 K^{-1} was assumed for the resistivity of the copper litz-wire. A finite element simulation with FEMM¹ was used to determine the self-inductances and the magnetic coupling for the prototype coil used in the experiments. An influence of the operating temperature on the IPT system can be observed, but it is small when compared to the effect of capacitance tolerances. This can be explained by the large air gap which mainly determines the reluctance of the arrangement, while the permeability of the core material has only a small influence. Additionally, the employed MKP film capacitors exhibit a comparably small temperature variance, while other types, e.g., MKN or MKT, would lead to a higher change in capacitance for increased temperatures.

III. EXISTING CONTROL METHODS

A block diagram of a typical IPT battery charging system is shown in **Fig. 4(a)**. A grid rectifier with Power Factor Correction (PFC) is to regulate the dc-link voltage $U_{1,dc}$, from which the IPT system is supplied. The IPT system is shown schematically in **Fig. 4(a)** as an inverter, a resonant circuit, and a rectifier on the receiver side. At the output of the rectifier, typically a dc-dc-converter is connected, which is used to control the battery current. An output filter is needed between the output of the dc-dc-converter and the battery to reduce the switching frequency ripple. For the regulation of the receiver-side dc-link voltage $U_{2,dc}$, from which the the dc-dc-converter is supplied, mainly the two different control methods that are discussed in the following are possible.

A. Control of the Switching Frequency

A typical control scheme for IPT systems is the frequency control method, where the transmitter-side inverter switching frequency is used as the actuating variable to regulate the output voltage $U_{2,dc}$ at the receiver-side. A possible implementation is shown in **Fig. 4(b)**, where the measured difference between $U_{2,dc}$ and its reference value $U_{2,dc}^*$ is fed to, e.g., a PI-controller. The controller continuously updates the inverter switching frequency f_{sw} from which the inverter switching signals $s_{1...4}$ are generated by a Pulse Width Modulation (PWM) module. An internal cross-check against a Safe Operating Area (SOA) is implemented in the PI controller to limit the switching frequency to the ZVS region of the resonant circuit that was either calculated or measured prior to operation. However, the switching conditions need to be constantly monitored and adapted, because the resonant frequency may differ from the anticipated value as discussed above.

B. Dual Control / Self-Sustained Oscillating Control

Alternatively, it is possible to determine the resonant frequency f_0 in real time, e.g., using a current transformer circuit and a comparator

¹Freeware, available at www.femm.info (3.3.2014).

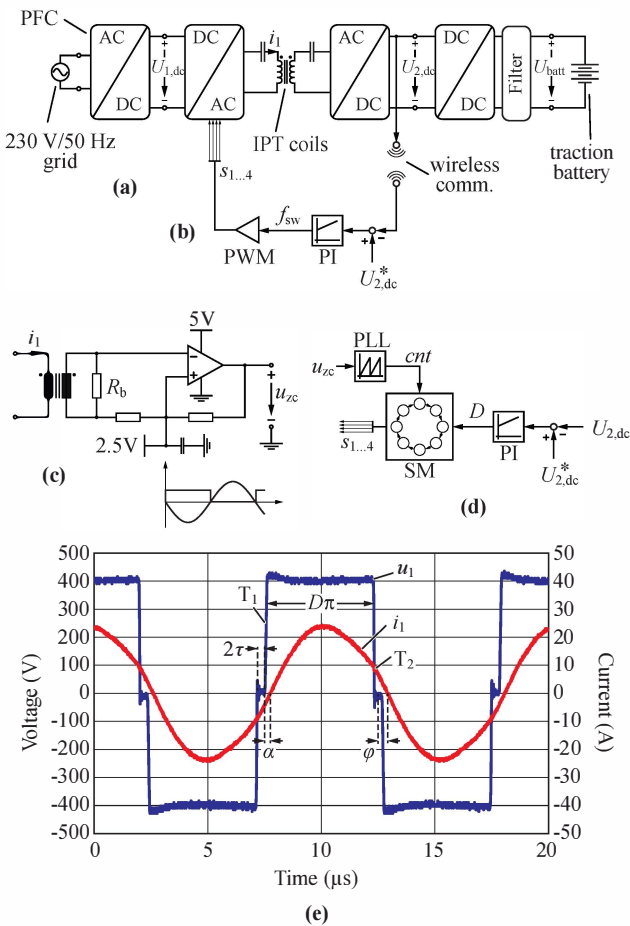


Fig. 4. (a) Block diagram of a series-series compensated IPT battery charging system that is supplied from the 230 V/50 Hz grid; (b) control diagram for the frequency control method; (c) zero crossing detection circuit; (d) control diagram for the dual control method; (e) measured waveform of the transmitter coil current i_1 and the transmitter-side inverter output voltage u_1 for the dual control method.

as shown in **Fig. 4(c)**. The comparator output voltage u_{zc} is used to trigger a Phase-Locked Loop (PLL) that synchronizes an internal counter to the zero crossings of the current in the transmitter coil. As shown in **Fig. 4(d)**, the PLL counter signal cnt is fed to a State Machine (SM) which generates the inverter switching signals $s_{1...4}$. Based on the zero crossing detection, it is possible to implement the dual control or self-sustained oscillating control method [16]–[18]. In this control scheme, the SM generates the switching signals such that the angular length $D\pi$ of the power interval as defined in the measured waveform in **Fig. 4(e)** can be adjusted by the PI-controller. Additionally, the angle α can be set such that the current during the switching transition T_1 is always sufficient to completely discharge the output capacitance of the MOSFET that is turned-on.

Instead of controlling the switching frequency directly, the angles $D\pi$ and α are controlled and the temporal duration of the individual inverter switching states are derived in real time from the PLL counter. Because the switching frequency is uncontrolled, the resonant system will autonomously converge to the frequency, where the phase of the input impedance $\arg[Z_{in}]$ (cf. **Fig. 2(c)**) is equal to the phase angle φ between the fundamental components of the voltage u_1 and the current i_1 . The resulting operating point is given approximately by

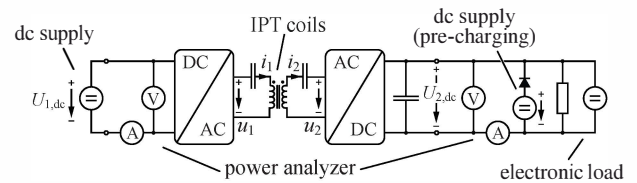


Fig. 5. Measurement setup used in the experiments.

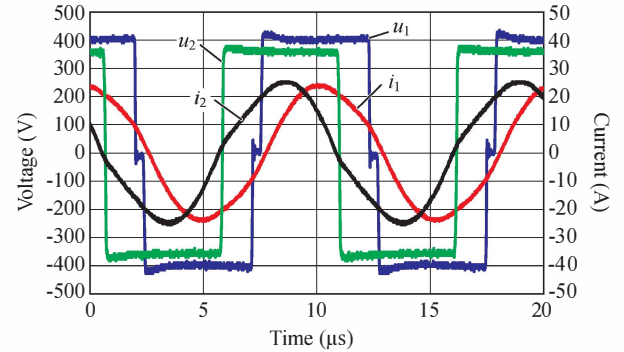


Fig. 6. Waveforms of a measurement at the transmission of 5.7 kW over an air gap of 52 mm. The efficiency at this operating point is 96.5%.

$$\varphi \equiv \underbrace{\frac{\pi}{2}(1-D)}_{\tau} + \alpha \equiv \arg[Z_{in}]. \quad (8)$$

This allows to account for variations of the resonant frequency due to component tolerances, temperature drift, or coil misalignment in an automatic fashion with guaranteed soft-switching in the ZVS region of the resonant circuit, which presents a fundamental advantage of the dual control method over the frequency control method [18].

An inherent disadvantage of both of the presented control methods is that the measured value of $U_{2,dc}$ has to be transmitted to the controller on the transmitter side via the wireless communication link. This introduces a time delay in the control loop and results in an increased reaction time of the output voltage regulation, which needs to be compensated by over-dimensioning of the passive components, e.g., the dc-link capacitance of the receiver.

C. Measured Performance of Existing Methods

The measurement setup that was used for these and all the measurements discussed in the following is shown in **Fig. 5**. A dc supply was used to set the transmitter-side dc-link voltage. For the regulation of the dc-link voltage at the receiver side, an electronic load in constant voltage mode was used. To dissipate the transmitted power, load resistors were used additionally to the electronic load. For the pre-charging of the receiver-side dc-link, another dc-supply was used, which is isolated by a series diode as soon as the power transmission is initiated.

Fig. 6 shows measured current and voltage waveforms in the resonant system at the transmission of the maximum output power of 5.7 kW. Waveforms for the dual control method with duty-cycle $D = 0.75$ (4.7 kW) and $D = 0.65$ (3.7 kW) are shown in **Fig. 7(a)**–**(b)**, respectively. A comparison of **Fig. 6** and **Fig. 7(b)** reveals a fundamental disadvantage of the dual control method (and also of the frequency control method): even though for the reduced output power the amplitude of the receiver coil current i_2 is lower, the amplitude of the current in the transmitter coil i_1 remains almost unchanged.

The calculated rms value of the current in the transmitter coil I_1 and the receiver coil current I_2 are shown in **Fig. 8(a)**–**(b)**,

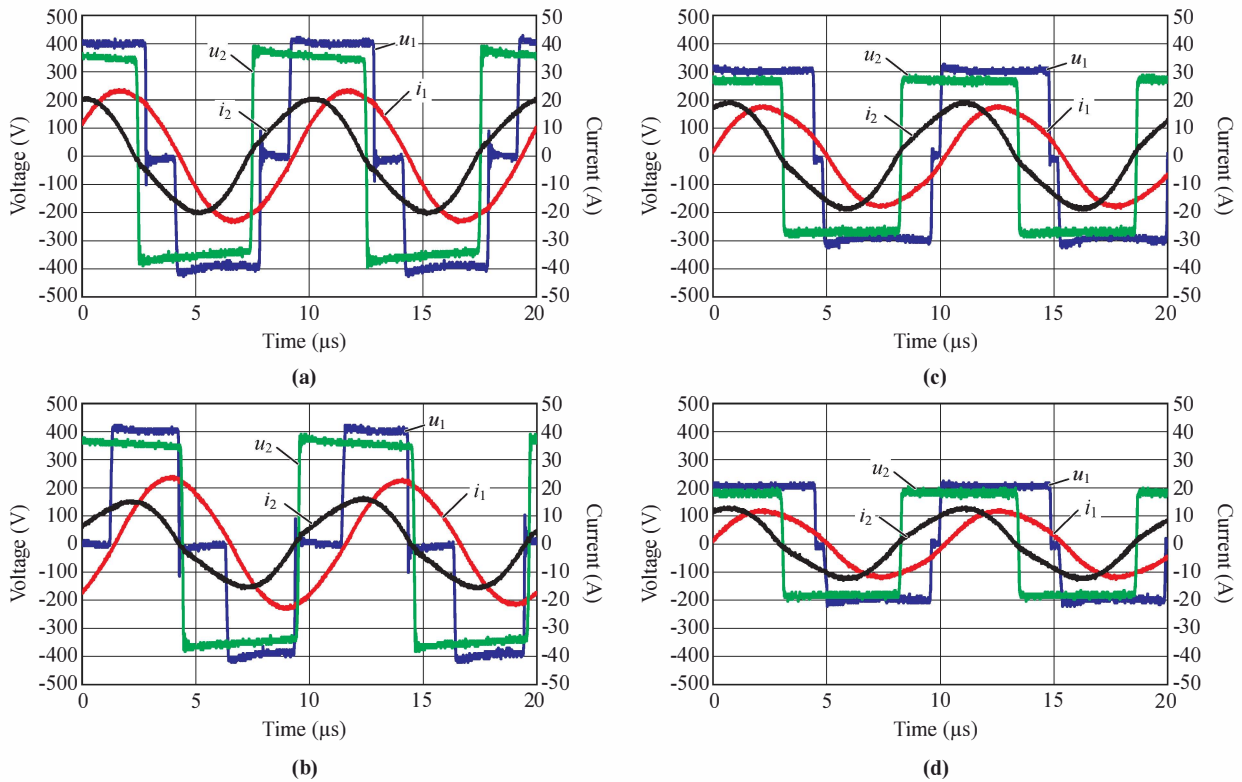


Fig. 7. (a)-(b) waveforms for the dual control method and duty-cycles $D = 0.75$ (4.7kW) and $D = 0.65$ (3.7kW), respectively; (c)-(d) waveforms at reduced output power with dc-link voltages controlled at $U_{1,dc} = 300\text{V}/U_{2,dc} = 265\text{V}$ (3.2kW) and $U_{1,dc} = 200\text{V}/U_{2,dc} = 176\text{V}$ (1.4kW).

respectively. For the dual control and the frequency control method, the rms value of the current in the transmitter coil is almost constant, while the current in the receiver coil is reduced. Consequently, the power loss in the transmitter coil also remains almost constant at reduced output power. The calculated power losses for the two control methods are shown in **Fig. 9(a)-(b)**. For the calculation of the power losses in the coils $P_{coil,1/2}$ a finite element tool was used as described in [2], [3]. The losses in the resonant capacitors $P_{cap,1/2}$ were estimated based on the manufacturer data given in [15]. For the power semiconductors $P_{semi,1/2}$, conduction losses were calculated based on the device datasheet. Because of the ZVS operation, no switching losses have to be included.

In partial-load, the losses in the transmitter coil $P_{coil,1}$, the transmitter-side resonant capacitor $P_{cap,1}$, and the transmitter-side power semiconductors $P_{semi,1}$ are almost equal for all values of the output power for the dual control and the frequency control method. This characteristic fundamentally impairs the efficiency of the system at reduced load. In order to overcome this limitation, a control method with an improved partial-load efficiency is presented in the next section.

IV. NOVEL CONTROL METHOD FOR HIGH-POWER IPT

As discussed in the previous section, while a deviation from the resonant frequency of the IPT system reduces the transmitted power, the current in the transmitter coil remains almost constant and, therefore, causes high losses in partial-load. A better performance can be achieved if the switching frequency is constantly at the resonant frequency of the IPT link and the two dc-link voltages $U_{1,dc}$ and $U_{2,dc}$ are used to control the output power [4]. For the series-series compensated IPT system, the relation

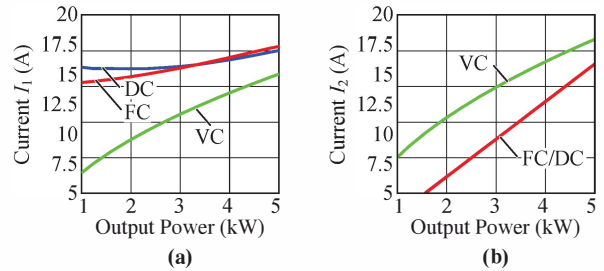


Fig. 8. (a) Calculated transmitter coil current I_1 and (b) receiver coil current I_2 for the frequency control (FC) method, the dual control (DC) method, and voltage control (VC) method (rms value).

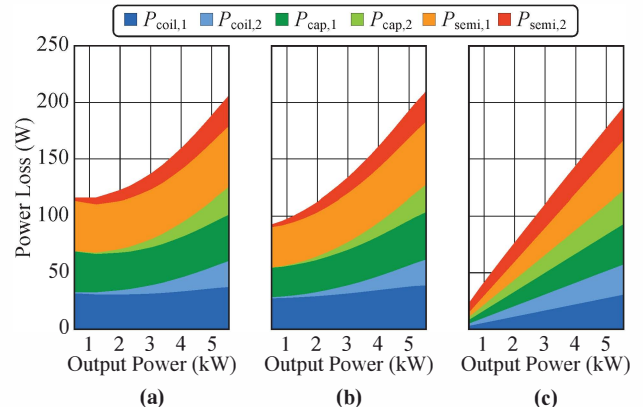


Fig. 9. Calculated power loss as a function of the output power for (a) the frequency control, (b) dual control, and (c) for the proposed voltage control method. Losses of the dc-dc-converter are not included.

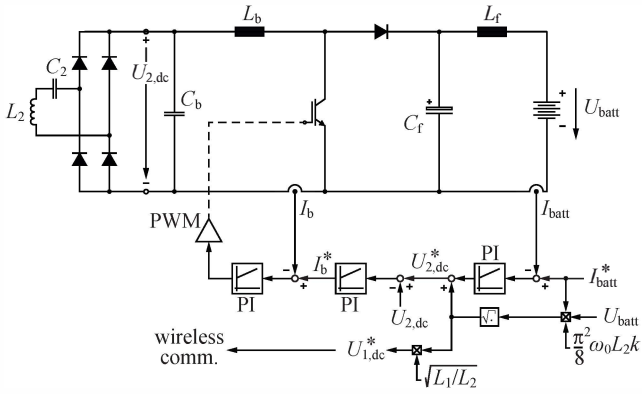


Fig. 10. Control diagram for the voltage control method. All critical parts are implemented within the receiver-side power electronic converter. The reference value $U_{1,dc}^*$ is the only inherently required communication with the transmitter that has to be transmitted across the air gap.

$$P_2 = \frac{8}{\pi^2} \frac{U_{1,dc} U_{2,dc}}{\omega_0 L_h} \quad (9)$$

holds for the output power P_2 of the IPT system. Therefore, if the dc-link voltages are controlled, the battery current can be regulated according to

$$I_{batt} = \frac{8}{\pi^2} \frac{1}{\omega_0 L_h} \frac{U_{1,dc} U_{2,dc}}{U_{batt}}, \quad (10)$$

since the battery is a voltage-impressing element and the battery current results from $I_{batt} = P_2/U_{batt}$.

In the following, a possible implementation is discussed in more detail and further improvements of the method for high-power IPT systems that employ IGBTs as switches are shown. Additionally, experimental results are presented that demonstrate the performance, which can be achieved with this control method.

A. Controller Implementation

An implementation of the described method is possible if the grid-side rectifier shown in **Fig. 4(a)** is realized as an active front-end that allows controlling the transmitter-side dc-link voltage or if an additional dc-dc-converter is implemented at the transmitter side. The receiver-side dc-link voltage can be regulated by the dc-dc-converter on the receiver side, which is also shown in **Fig. 4(a)**.

The condition for the maximum efficiency of the IPT system is that the receiver reactance is matched to the equivalent load resistance (3) according to (1). Hence, if the receiver-side dc-link voltage can be controlled according to

$$U_{2,dc}^* = \sqrt{\frac{\pi^2}{8} \omega_0 L_2 k P_2}. \quad (11)$$

at reduced output power, the equivalent load resistance is maintained constant and the matching condition is always fulfilled. Therefore, this process could be termed *active impedance matching*. Note that if the equivalent load resistance is maintained constant independently of the output power, the strong load-dependency of the transfer characteristics of the series-series compensated IPT system described, e.g., in [19], is eliminated.

Because of the symmetry of (9), it is sufficient if a feedback controller is used to adapt one of the reference values dynamically to compensate inaccuracies in the analytical calculation shown above. **Fig. 10** shows a possible configuration, where the reference value $U_{2,dc}^*$ is manipulated by a PI-controller to regulate the battery current.

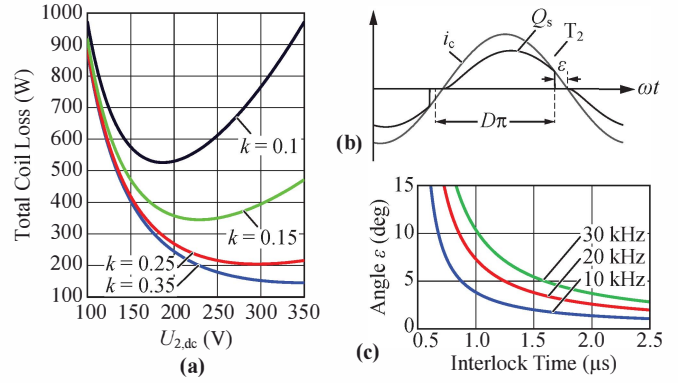


Fig. 11. (a) Coil losses as a function of the secondary-side dc-link voltage $U_{2,dc}$ and the magnetic coupling k (coil misalignment); (b) schematic waveforms of IGBT collector current i_c and stored charge Q_s ; (c) turn-off angle ϵ for minimum IGBT soft-switching losses as a function of the interlock time and the transmission frequency.

Also the cascaded control loop for the receiver-side dc-link voltage is shown. Note that **Fig. 10** shows a boost topology for the dc-dc-converter mainly as an example. Depending on the battery voltage and the rating of the employed power semiconductors, also a buck-boost-type converter could be used.

The reference value for the dc-link voltage $U_{1,dc}$ follows from (2) as

$$U_{1,dc}^* = \sqrt{\frac{L_1}{L_2}} U_{2,dc}^*. \quad (12)$$

The reference value $U_{1,dc}^*$ is sent through, e.g., a wireless communication channel to the power electronic converter on the transmitter side, where another, local PI-controller regulates the voltage. It is also possible to adapt $U_{1,dc}^*$ with the PI-controller instead of $U_{2,dc}^*$. However, then the reaction time of the battery current control loop would be lower, due to the delay that is introduced by the communication across the air gap. In the proposed configuration, all critical parts of the battery charging control are implemented on the receiver, which has a more direct access to the measurements. This is considered the inherently safest and most reliable design.

B. Tracking of the Efficiency Maximum with Misalignment

To calculate the reference values (11) and (12) accurately, an estimate of the magnetic coupling is needed. If a feedback controller is used, also a pre-calculated, approximative value can be used and the control would be compensated for the estimation error. However, ideally a method is implemented to estimate the magnetic coupling in real time, e.g., from measurements of the currents in the IPT coils and an equivalent circuit.

If an estimate is available, the reference value $U_{2,dc}^*$ can be adapted to the magnetic coupling in real time to follow the loss minima shown in **Fig. 11(a)**, which are described by (11). Alternatively, it is also possible to measure the dc input and output power of the system and calculate the power loss online. An optimization algorithm or a look-up table could then be used to determine reference values that lead to minimum total losses in the system.

C. Control of IGBT Soft-Switching Conditions

If the circuit for the detection of the zero crossings and the PLL discussed in Section III for the dual control method are also implemented for the voltage control scheme, another valuable advantage arises: it was shown in [7]–[10] that the stored charge of IGBTs causes high switching losses, even if they are commutated with

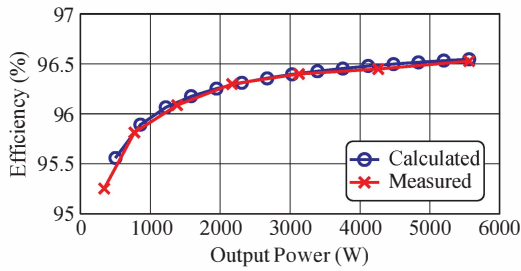


Fig. 12. Calculated and measured dc-to-dc conversion efficiency (incl. losses in the IPT coils, resonant capacitors, and power semiconductors) as a function of the output power at an air gap of 52 mm, using the voltage control method.

almost zero current. For IPT systems with a high power level, e.g., several tens of kW, for all of the discussed control methods this effect could severely impair the performance, because the IGBTs are always switched close to the zero crossings of the current. Novel SiC modules with better switching performance are often proposed to circumvent this problem, e.g. in [4]. However, due to their high reliability, low cost, and better availability at present time IGBT modules are still clearly preferred in industry. The possibility to minimize the effect of the stored charge, which is discussed in the following is, therefore, a key advantage of the proposed voltage control scheme.

In [9], it was shown that an optimum exists for the current during the turn-off transition of an NPC-bridge leg operated in discontinuous conduction mode in a solid state transformer application. The optimally switched current is given where the charge that is removed from the IGBT by the magnetizing current of the transformer during the zero current interval is equal to the stored charge in the junction of the IGBT, because the turn-on losses of the complementary device are eliminated and the total losses reach a minimum.

Similarly, for the schematically reproduced waveforms of the IPT system in **Fig. 11(b)**, a condition for minimum IGBT switching losses follows for the turn-off angle ϵ . At the switching transition T_2 , the charge that is removed from the IGBT by the collector current i_c during the interlock time must be equal to the charge Q_s that is stored in the IGBT junction in order to completely eliminate the turn-on losses of the complementary device. Under the assumption of a sinusoidal current in the transmitter coil and with the stored charge model discussed in [8], [9], the optimum angle ϵ can be calculated numerically. In **Fig. 11(c)** the optimum is shown as a function of the interlock time and for different switching frequencies. It can be seen that for higher switching frequencies a higher angle ϵ is needed to completely remove the charge from the IGBT, which is still higher at the turn-off due to the time constant of the device.

With the zero crossing detection and the PLL, the switched current during the transition T_2 can be controlled by adjusting the angle $D\pi$ in combination with the described control voltage method. If the voltages can be adjusted within a sufficient range, the angle $D\pi$ is an additional degree of freedom of the control method. This allows to minimize the IGBT switching losses significantly by tracking the discussed optimum for the turn-off angle ϵ . This optimization is not possible with the existing control methods that were described in Section III, since there, the phase shift between current and voltage is needed for the power control and is, therefore, not available for another control loop.

D. Measured Performance of the Voltage Control Method

Measured waveforms at two power levels are shown in **Fig. 7(c)-(d)**. The calculated rms currents that results in the transmitter and

receiver coil are indicated in **Fig. 8(a)-(b)**, respectively. The current in the transmitter coil can be significantly reduced due to the reduction of the dc-link voltages at lower output power. The current in the receiver coil is slightly increased, but this is needed to drive the system to the global loss optimum, which is also evident from the calculated power losses shown in **Fig. 9(c)**.

Using a Yokogawa WT3000 power analyzer, the dc-to-dc efficiency of the system was measured for different load points. The results of the efficiency measurement at an air gap of 52 mm are shown in **Fig. 12**. As indicated, the measured and calculated performance show an excellent agreement, which validates the used methods.

A more detailed discussion of the used IPT prototype system and the measurement setup can be found in [2], [3], where also thermal and stray field measurements are presented to verify the finite-element based models. In the experiments, the dc-link voltages were adjusted with the dc-supply and the electronic load shown in **Fig. 5**. In a practical system, this would be the task of the dc-dc-converters. However, it is expected that the outcome of the measurements would be the same.

As confirmed by the measurements, the proposed voltage control methods shows an excellent performance, that can not be reached with the existing control methods. However, the price that has to be paid is the additional losses and the volume of the dc-dc-converter that is required on the transmitter side of the system.

V. REQUIREMENTS FOR THE ADDITIONAL DC-DC-CONVERTER

Generally, it can be considered an advantage of the proposed solution that power losses can be shifted from the IPT coils to the power electronic converters, since an efficient cooling of the IPT coils is more complex than the cooling system of a power electronic converter. Due to the stray field of the coils, high eddy current losses would occur in any metal parts. Therefore, the copper windings and the core materials of the IPT coils would need to be mechanically fixed mostly with plastic components, which typically have a comparably low thermal conductivity. The cooling would need to be provided either passively, or by forced air from integrated fans or a compressed air supply. Meanwhile, the components of the power converter could be mounted on a standard heatsink, which could be forced air cooled or even connected to a water-cooling circuit of the EV, which would allow for a highly compact and robust realization [20], [21]. Nevertheless, the over-all system efficiency is still an important performance aspect. Therefore, requirements of the dc-dc-converter are derived in the following.

For the topology shown in **Fig. 13(a)** and equal, bi-directional dc-dc-converters with efficiency $\eta_{\text{dc/dc}}(P_2)$, for the proposed voltage control method

$$\eta_{\text{dc/dc}}(P_2)^2 \cdot \eta_{\text{VC}}(P_2) \dots \geq \max[\eta_{\text{FC}}(P_2), \eta_{\text{DC}}(P_2)] \cdot \eta_{\text{dc/dc}}(P_2) \quad (13)$$

must apply to outperform the frequency control and the dual control methods. In (13), $\eta_{\text{VC}}(P_2)$ is the efficiency of the voltage control method as a function of the output power P_2 , while $\eta_{\text{FC}}(P_2)$ and $\eta_{\text{DC}}(P_2)$ are the efficiencies of the frequency control and dual control methods, respectively.

It is assumed that for the frequency control and the dual control methods, a dc-dc converter is implemented on the receiver side to control the battery current locally, which is not strictly needed, but advisable and commonly used for the protection of the battery. Then, the required efficiency of the dc-dc-converter is given as

$$\eta_{\text{dc/dc}}(P_2) \geq \frac{\max[\eta_{\text{FC}}(P_2), \eta_{\text{DC}}(P_2)]}{\eta_{\text{VC}}(P_2)} \quad (14)$$

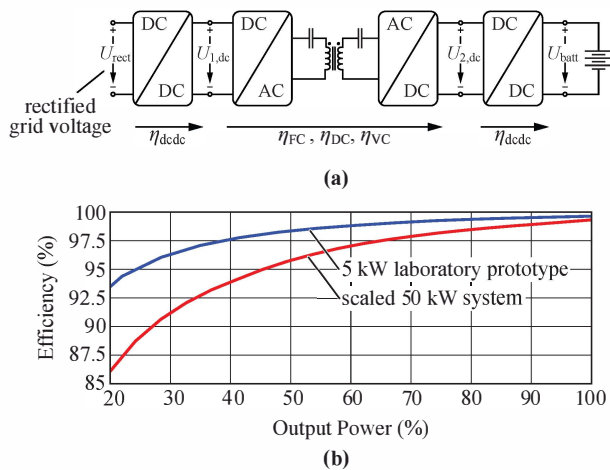


Fig. 13. (a) Considered system topology for the derivation of the efficiency requirement for the dc-dc-converters; (b) required minimum efficiency as a function of the output power for the 5 kW laboratory prototype with MOSFETs and a scaled 50 kW high-power IPT system that incorporates 1.2 kV IGBTs.

As shown in **Fig. 13(b)**, for a scaled 50 kW high-power IPT system, which incorporates IGBTs, a large loss reduction is possible with the proposed control method, and the efficiency requirement for the dc-dc-converter is feasible. Particularly, if a modular converter system as shown in [20], [21] is implemented, a high partial-load efficiency is possible if the modules are sequentially activated and deactivated, depending on the output power. For the 5 kW laboratory prototype, where MOSFETs are employed in the IPT system and no switching losses occur due to ZVS, the required efficiency is higher and a realization of the converter is more challenging. However, considering state-of-the-art dc-dc-converters also this task seems achievable [22].

VI. CONCLUSION

In this paper, the two existing control schemes frequency control and dual control are analyzed and compared in detail, using both calculations and measurements. It is shown that a significant disadvantage of both methods is the high reactive current in the transmitter coil during phases of reduced output power and, therefore, high partial-load losses in the transmitter coil.

Based on the results, a novel control method with significantly lower losses in partial-load is derived, where the dc-link voltages on both sides of the IPT system are regulated by dc-dc-converters to control the output power. The novel method includes the zero crossing detection of the dual control method, which allows full control of the power semiconductor switching conditions. It, therefore, enables the minimization of IGBT soft-switching losses, since the output current during the switching transition is an additional degree of freedom of the control. Experimental results demonstrate the excellent performance of the proposed novel method.

The price for the good results is an additional dc-dc-converter, for which the requirements are also derived. Assuming a state-of-the-art converter with 99% efficiency, and given the experimentally verified 96.5% transmission efficiency of the described prototype IPT system, a total conversion efficiency from grid to battery of 95% is expected with the proposed control method, even for high-power systems that incorporate IGBTs.

ACKNOWLEDGMENT

The authors would like to thank ABB Switzerland Ltd. for their funding and for their support regarding many aspects of this research project.

REFERENCES

- [1] E. Waffenschmidt and T. Staring, "Limitation of inductive power transfer for consumer applications," in *Proc. 13th European Conf. on Power Electronics and Applications (EPE)*, 2009, pp. 1–10.
- [2] R. Bosshard, J. W. Kolar, and B. Wunsch, "Accurate finite-element modeling and experimental verification of inductive power transfer coil design," in *Proc. 29th Appl. Power Electronics Conf. and Expo. (APEC)*, 2014.
- [3] R. Bosshard, J. W. Kolar, J. Mühlethaler, I. Stevanovic, B. Wunsch, and F. Canales, "Modeling and η - α -Pareto optimization of inductive power transfer coils for electric vehicles," *IEEE J. Emerg. Sel. Topics Power Electron.* (accepted for publication), 2014.
- [4] B. Goeldi, S. Reichert, and J. Tritschler, "Design and dimensioning of a highly efficient 22 kW bidirectional inductive charger for e-mobility," in *Proc. Int. Exhibition and Conf. for Power Electronics (PCIM Europe)*, 2013, pp. 1496–1503.
- [5] U. K. Madawala and D. J. Thrimawithana, "A bidirectional inductive power interface for electric vehicles in V2G systems," *IEEE Trans. Ind. Electron.*, vol. 58, no. 10, pp. 4789–4796, 2011.
- [6] R. M. Miskiewicz, A. J. Moradewicz, and M. P. Kazmierkowski, "Contactless battery charger with bi-directional energy transfer for plug-in vehicles with vehicle-to-grid capability," in *Proc. IEEE Int. Ind. Electron. Symp. (ISIE)*, 2011, pp. 1969–1973.
- [7] P. Ranstad and H.-P. Nee, "On dynamic effects influencing IGBT losses in soft-switching converters," *IEEE Trans. Power Electron.*, vol. 26, no. 1, pp. 260–271, 2011.
- [8] G. Ortiz, H. Uemura, D. Bortis, J. W. Kolar, and O. Apeldoorn, "Modeling of soft-switching losses of IGBTs in high-power high-efficiency dual-active-bridge dc/dc converters," *IEEE Trans. Electron Devices*, vol. 60, no. 2, pp. 587–597, 2013.
- [9] J. Huber, G. Ortiz, F. Krismer, N. Widmer, and J. W. Kolar, " η - ρ -Pareto optimization of bidirectional half-cycle DC/DC converter with fixed voltage transfer ratio," in *Proc. 28th Appl. Power Electronics Conf. and Expo. (APEC)*, vol. 1, 2013, pp. 1413–1420.
- [10] D. Dujic, G. K. Steinke, M. Bellini, M. Rahimo, L. Storasta, and J. K. Steinke, "Medium-Frequency Soft-Switched Applications," *IEEE Trans. Power Electron.*, vol. 29, no. 2, pp. 906–919, 2014.
- [11] R. Steigerwald, "A comparison of half-bridge resonant converter topologies," *IEEE Trans. Power Electron.*, vol. 3, no. 2, pp. 174–182, 1988.
- [12] P. E. K. Donaldson, "Frequency hopping in r.f. energy-transfer links," *Electronics & Wireless World*, pp. 24–26, Aug. 1986.
- [13] C.-S. Wang, G. A. Covic, and O. H. Stielau, "Power transfer capability and bifurcation phenomena of loosely coupled inductive power transfer systems," *IEEE Trans. Ind. Electron.*, vol. 51, no. 1, pp. 148–157, 2004.
- [14] EPCOS, "Ferrites and accessories - data handbook," 2006.
- [15] —, *Film capacitors - data handbook*, 2009.
- [16] J. A. Sabate, M. M. Jovanovic, F. C. Lee, and R. T. Gean, "Analysis and design-optimization of LCC resonant inverter for high-frequency AC distributed power system," *IEEE Trans. Ind. Electron.*, vol. 42, no. 1, pp. 63–71, 1995.
- [17] H. Pinheiro, P. K. Jain, and G. Joos, "Self-sustained oscillating resonant converters operating above the resonant frequency," *IEEE Trans. Power Electron.*, vol. 14, no. 5, pp. 803–815, 1999.
- [18] R. Bosshard, U. Badstübner, J. W. Kolar, and I. Stevanovic, "Comparative evaluation of control methods for inductive power transfer," in *Proc. 1st Energy Research and Applicat. Conf. (ICRERA)*, vol. 1, no. 1, 2012, pp. 1–6.
- [19] I. Nam, R. Dougal, and E. Santi, "Optimal design method to achieve both good robustness and efficiency in loosely-coupled wireless charging system employing series-parallel resonant tank with asymmetrical magnetic coupler," *Proc. 5th Energy Conversion Congr. and Expo. (ECCE USA)*, pp. 3266–3276, 2013.
- [20] B. Eckardt and M. März, "A 100kW automotive powertrain DC/DC converter with 25kW/dm³ by using SiC," in *Proc. Int. Exhibition and Conf. for Power Electronics (PCIM Europe)*, 2006.
- [21] S. Waffler and J. Kolar, "Efficiency optimization of an automotive multi-phase bi-directional DC-DC converter," in *Proc. 6th Int. Power Electron. and Motion Control Conf. (ECCE Asia)*, 2009, pp. 566–572.
- [22] J. W. Kolar, F. Krismer, Y. Lobsiger, J. Mühlethaler, T. Nussbaumer, and J. Miniböck, "Extreme efficiency power electronics," in *Proc. 7th Int. Conf. Integrated Power Electron. Syst. (CIPS)*, 2012, pp. 1–22.